CONF-8910222--7

DE90 003705

IMPROVED EDDY-CURRENT INSPECTION FOR STEAM GENERATOR TUBING*

C. V. Dodd, J. R. Pate and J. D. Allen, Jr.

Oak Ridge National Laboratory
P.O. Box 2008, Oak Ridge, TN 37831-6158

ABSTRACT

Computer programs have been written to allow the analysis of different types of eddy-current probes and their performance under different steam generator test conditions. The probe types include the differential bobbin probe, the absolute bobbin probe, the pancake probe and the reflection probe. The generator test conditions include tube supports, copper deposits, magnetite deposits, denting, wastage, pitting, cracking and IGA. These studies are based mostly on computed values, with the limited number of test specimens available used to verify the computed results. The instrument readings were computed for a complete matrix of the different test conditions, and then the test conditions determined as a function of the readings by a least-squares technique. A comparison was made of the errors in fit and instrument drift for the different probe types. The computations of the change in instrument reading due to the defects have led to an "inversion" technique in which the defect properties can be computed from the instrument readings. This has been done both experimentally and analytically for each of these probe types.

Measurements and computations were also made of the effect of sampling rate on the accuracy of the defect depth measurement for the bobbin probe. For simple defect signals, a relatively coarse sample rate is sufficient to determine the defect depth. The frequency response of the signal produced as the coil is scanned past the defect determines the desired response of the instrument amplifiers.

Neural networks have been applied to the analysis of eddy-current defect signals in the presence of other signals, such as tube supports, magnetite deposits, and copper deposits. These networks are used on unmixed data and have worked very well for the limited data sets evaluated thus far.

COMPUTER CODE FOR EDDY-CURRENT ANALYSIS

ORNL has written and maintained computer codes for the solution of general eddy-current problems for a number of years. These programs have been updated for use on the PC-AT Clone computers and modified specifically for steam generator-related problems. Many of the new programs have been collected and incorporated into a report with instructions for their use and examples of the computer runs.[1] Programs have been written to analyze the probe types shown in Figure 1. These include the differential bobbin probe, which is the most common type of probe used for steam generator tests. The problem of the absolute bobbin probe is very

---

* Research sponsored by the Office Nuclear Regulatory Research, Division of Engineering, U.S. Nuclear Regulatory Commission under Interagency Agreement DOE 1886-8041-7B with the U.S. Department of Energy under Contract DE-AC05-840R21400 with Martin Marietta Energy Systems, Inc.

[1] J. R. Pate and C. V. Dodd, *Computer Programs For Eddy-Current Defect Studies*, ORNL/TM in progress, 1989.

similar, and a second set of programs performs the computations for this problem. The pancake probe, which has many features contributing to a very significant increase in signal-to-noise ratio over the bobbin probe, is also included. The pancake coil inspects a smaller volume of tube than the bobbin coil and exhibits increased sensitivity at the expense of longer inspection times. The reflection coil exhibits still better performance than the pancake coil but is more complex to manufacture and more expensive.

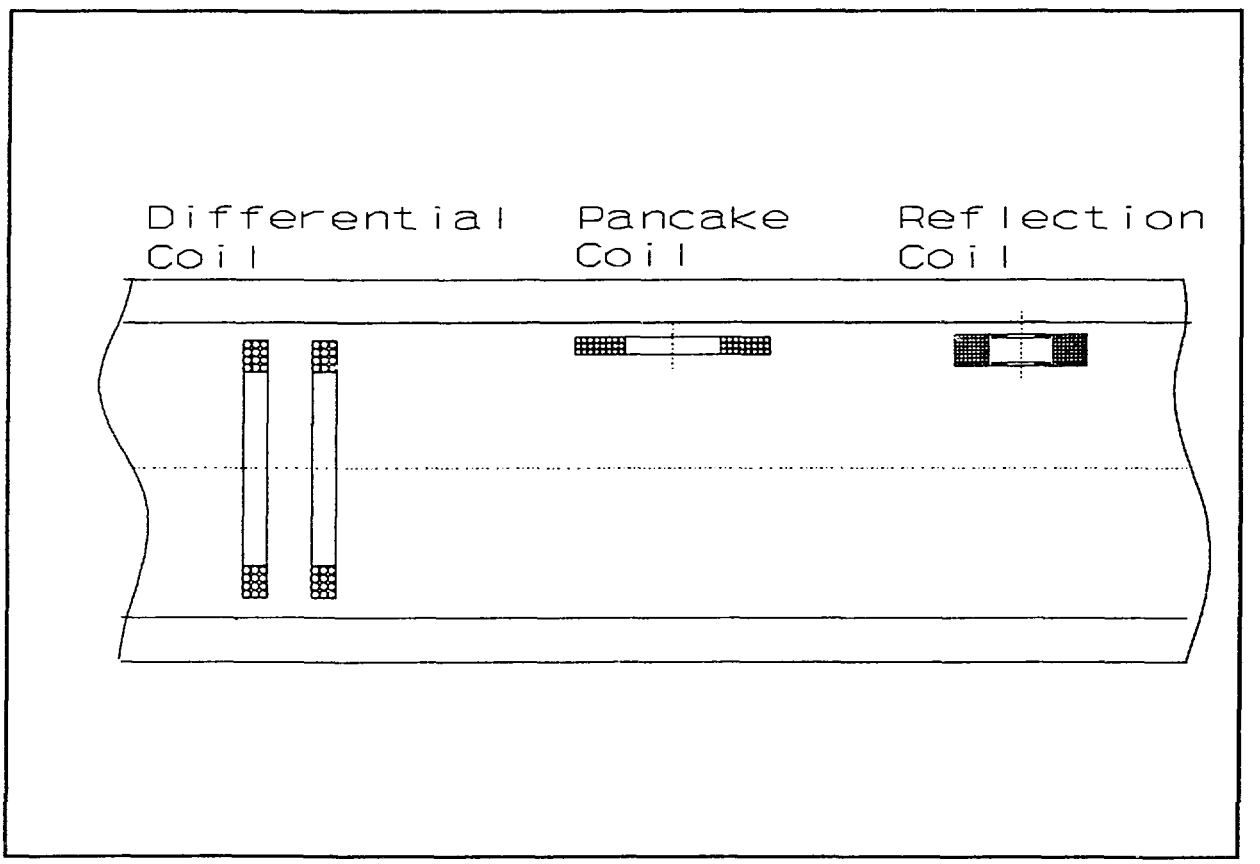

Figure 1 Bobbin probes (absolute and differential), pancake probes and reflection probes are used for eddy-current tests

These probes include most common types used in steam generator inspections. The programs are written to compute the coil impedances or coil voltages and calculate the changes produced as the probe is scanned past a point defect. The point defect can be averaged over depth or volume to approximate a finite sized defect. The response to a defect can be approximated by a defect sensitivity factor multiplied by the volume of the defect. Some of the programs calculate the defect sensitivity factor for an array of defect locations located around the coil and plot contours of the magnitude and phase of the defect sensitivity factor. This is very useful in visualizing the field pattern of a coil system and the response of a defect at various locations throughout the tube wall. Additional programs perform the direct computation of the volume and depth of the defect from the magnitude and phase of the signal as the probe scans across the defect.

DETERMINATION OF DEFECT SENSITIVITY FACTOR FOR PROBES

As an example we have calculated the defect sensitivity factor for a differential bobbin probe. In Figure 2 we show the magnitude of the defect sensitivity factor for the entire probe.

The signal is zero when the defect is far from the probe, increases to a maximum value when the defect is close to the center of the windings of the first coil, and goes to zero again when the defect is located exactly between the two coils. The signal has an anti-symmetrical response as the defect moves past the second coil, reaching a minimum near the center of the windings on the second coil and then increasing to zero as the defect moves far from the probe. One can think of the phase shifting by 180 degrees as the defect passes the probe center, or the amplitude going from positive to negative. The latter convention seems to make the problem easier to explain. The response to the defect is symmetrical with respect to either coil if the coils are far apart, but because the coils are in opposition and the defect signal from each coil is subtracted from the other, the response between the coils is skewed, with the maximum signal shifting toward the outer edge of each coil.

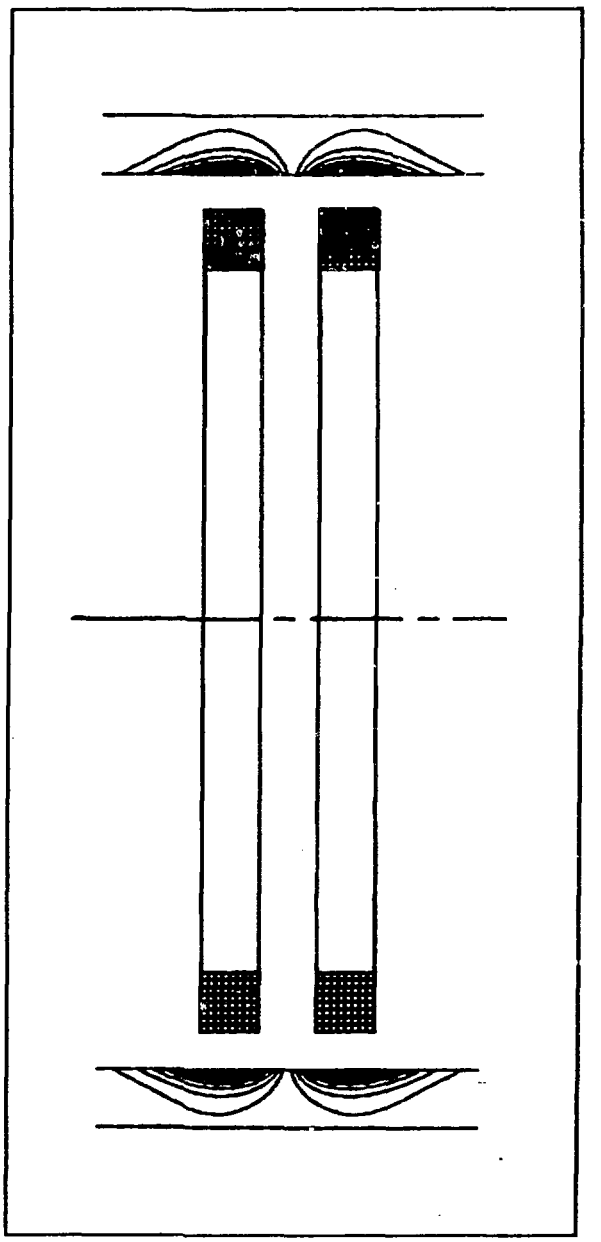

Figure 2 Magnitude contours of the defect sensitivity factor for a differential bobbin probe. These contours represent the magnitude of the impedance change due to a point defect at different locations in the tube wall.

Because of the symmetry of the coil and conductor in Figure 2, the same information is repeated in each of the four quadrants. Thus the behavior can be more clearly represented by a plot of magnitude of the defect sensitivity factor in only the upper left quadrant, as shown in Figure 3. This plot gives more detail than was available in the previous figure. The dotted line represents the probe center where the magnitude has decreased to zero. Since the defect sensitivity factor is a complex quantity with both magnitude and phase, we can also plot the phase as shown in Figure 4. The phase shift increases with distance into the tube and remains relatively constant with distance along the tube. This phase shift increase with distance into the tube is the main contribution to the phase shift with defect depth observed in our eddy-current tests. The phase shift when the

magnitude of the signal approaches zero at the probe center is undefined. If we adopt the convention that the amplitude changes sign as the defect passes the center of the probe, the phase has the same value on the opposite side and a smooth transition between. Otherwise, it would vary by 180 degrees as the defect passed the center, giving a discontinuous shift in the phase.

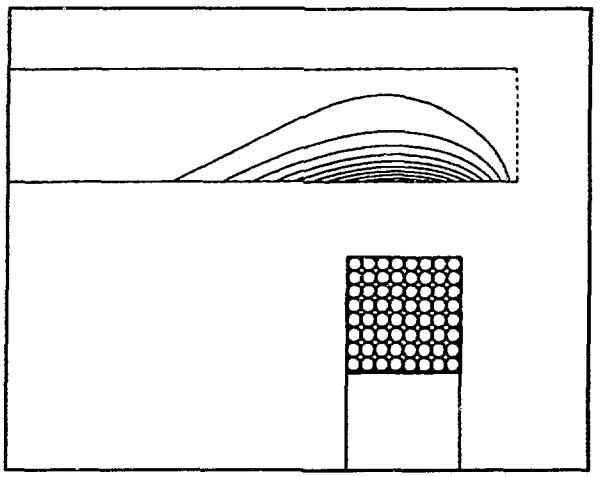

Figure 3 Magnitude contours of the defect sensitivity factor for one quadrant of a differential bobbin probe

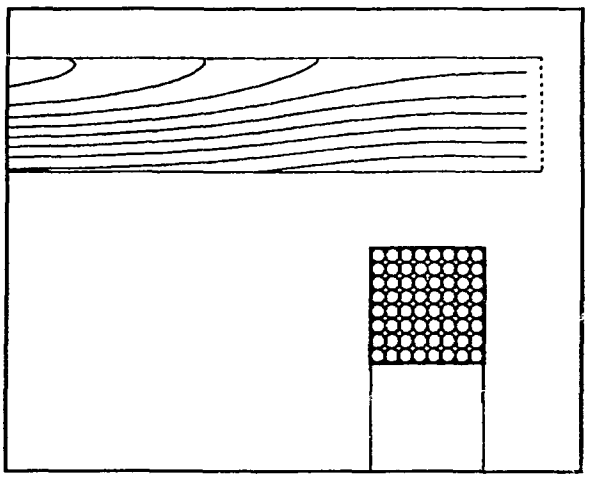

Figure 4 Phase contours of the defect sensitivity factor

From the shape of the defect sensitivity factor curves, we can see how the probe would respond to a small defect anywhere within the metal. These plots show how the sensitivity to a small defect falls off as the defect approaches the tube outer surface and show the volume of metal that is being inspected by the probe. Defect sensitivity factor curves for the pancake and reflection probes fall off much more rapidly with distance into the metal. They are less sensitive to property variations on the outer surface of the conductor, such as copper deposits, magnetite deposits, or tube supports. They also are sensing a smaller volume of material at one time and so are still sensitive to small defects on the outer surface. On the other hand, due to their relatively small size, they are more sensitive to spacing variations between the coil and metal. Therefore their liftoff must be controlled by mechanical means or by electronic compensation. For best results, a combination of the two is necessary.

MINIMIZATION OF SYSTEM ERRORS

Various probe systems can be compared for different conditions and property variations using ORNL-developed multiple property techniques. If we have a set of property variations for a given eddy-current test, we can either measure or calculate the response of our eddy-current instrument for each possible combination of the test properties. In general, the calculations are performed first since they can be made quickly and cheaply, particularly compared to the cost of constructing accurate standards and making experimental measurements. Later, when a good system design is achieved, we can construct the probe, standards, and instrument and make the measurements experimentally, since we are not generally able to construct the probe to the accuracy needed to use the same calibration coefficients.

Then, since we know both the instrument readings and the initial test properties, we can calculate a set of least-squares coefficients to relate the properties to the readings. Due to the nonlinearity of eddy currents, it is generally better to use a polynomial function of the readings rather than the readings directly. This does not affect the least-squares process and yields a much better fit between the readings and the properties.

The properties can then be recomputed using the coefficients and compared to the original set of properties with which we started. The difference between these two sets is called the fit error. In addition to the fit error, there is a second error known a drift error. Since all instrument measurements have some error, we vary each individual reading by the maximum amount that the instrument can drift, and compute the change in the property. The absolute sum of the individual errors is called the drift error. An rms sum of the drift error and the fit error gives us a good measure of how accurately we can perform a given inspection. We can also vary the coil design, operating frequency, instrument design, the degree and type of instrument reading polynomial, and in some cases, the sets of property variations that we will allow. Comparisons can be made of the error present in the various tests, and the best compromises can be chosen. In general, the best system design will have fit and drift errors of about the same size. In Figure 5 we show how the error in calculation of the defect size varies with coil mean radius for pancake and reflection probes.

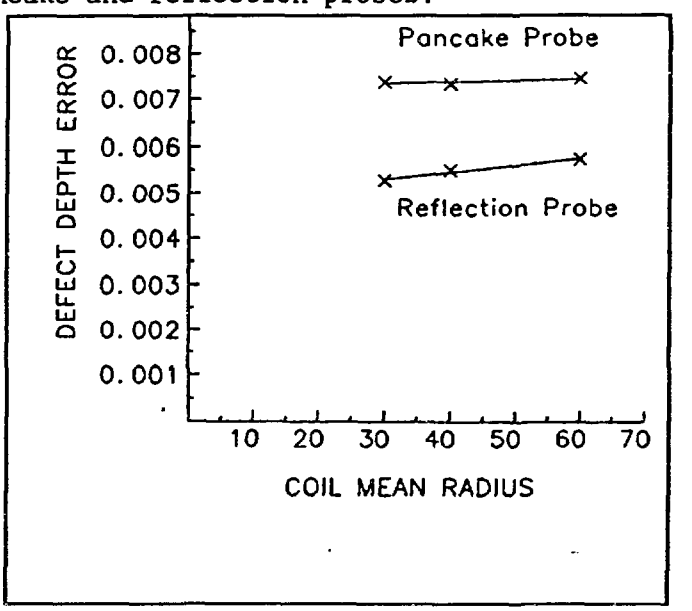

Figure 5 Defect depth measurement error for a reflection probe and a pancake probe plotted against probe mean radius

We can see that the reflection probe gives a more accurate measurement of the defect depth for this particular set of properties. We can also see that the measurement error is relatively constant with probe size. The error due to liftoff variation decreases as the probe size is increased but is offset by an increase in errors due to property variations on the outside of the tube. The pancake coil error reaches a minimum at a mean radius of 0.040 in., while the reflection probe error reaches a minimum at a smaller mean radius. Usually a second factor, such as the amount or coverage of the tube, will force a compromise to be made. In order to achieve adequate coverage of a tube with 0.875 in. diameter with an array of sixteen coils, the probe mean radius needs to be about 0.040 in. The sensitivity increases very little for smaller sized reflection probes.

A set of coefficients is obtained for each property we wish to calculate, and that set of coefficients multiplied by the readings extract that particular property, even in the presence of the variation of all of the other properties. This overall technique is very general and will work for any type of instrument readings and set of properties. It has been applied successfully to a number of complex eddy-current test problems in addition to the steam generator

problems. The instrument readings that have been used were both multiple frequency and pulsed. Data from other types of NDE tests can also be used as the instrument readings, although this technique has not been widely applied outside of eddy-current tests as of this date.

As an example of the polynomial fit optimization process for a given system, defect depth error data were determined for 780 different combinations of properties with a second order reading polynomial for the magnitude and phase and a cross term between the magnitude and phase. Thus, there were as many as five reading terms for each frequency. In general, the defect accuracy increases for higher order polynomial fits and decreases as more properties are added to the set. For an increase to a third degree polynomial, the fit error decreased by about 20%. Since, for this problem, the fit error was considerably larger than the drift error, the rms error also decreased by about 20%. On the other hand, the number of possible combinations of polynomials and the time required to calculate all of them is increased by a factor of 27. A computer program is used to find the best polynomial fit for each simultaneous combination of three operating frequencies. The frequencies are selected from a set of six frequencies, and only the best fit and the lowest rms error are printed out for each three-frequency combination. Most of the preliminary design is done with second order polynomial approximations and for a relatively small number of property sets until we approach a final design. Then the longer running studies with higher degree polynomials and larger sets of properties can be performed.

SAMPLE RATE STUDY

Another application of the use of our computer codes has been for a sample rate study.[2] The study was initiated to resolve questions about a proposed modification of the inspection code. In the study, both the rate of sampling as the tube was scanned and the instrument frequency response were investigated. The study consisted of both experimental measurements made on ASME Section XI standard defects using a Zetec MIZ17 and the computed effects of a point defect. The ASME defects are much longer than a point defect so that the latter represents the limiting case for both the sample rate and frequency response studies. In Figure 6 we show the magnitude of the defect signal as we scan across both a point defect and the ASME Section XI 40% defect. Note that the point defect response is concentrated in a smaller distance along the tube than the experimental defect. The convention of the magnitude changing signs has been followed in Figure 6 so that the phase shift is relatively constant with distance along the tube.

If we assume a constant probe speed, the defect signal has a given frequency response. For purposes of this plot, we have assumed a constant inspection speed of one foot per second. This is the standard inspection speed used in most generator inspections in the US with a differential bobbin probe. In Figure 7 we show the frequency response of two defect signals. We have taken the Fourier transform of the complex defect signal, so that any phase variations in the defect signal are included in the frequency response. Note that the point defect has a higher frequency response than the experimental defect and represents the upper limit of the defect response. The experimental defect also has a long tail

---

[2] C. V. Dodd, *Effects of Sampling Rate on Eddy-Current Measurements*, Oral Presentation at ASME meeting, Salt Lake City, January 16, 1989.

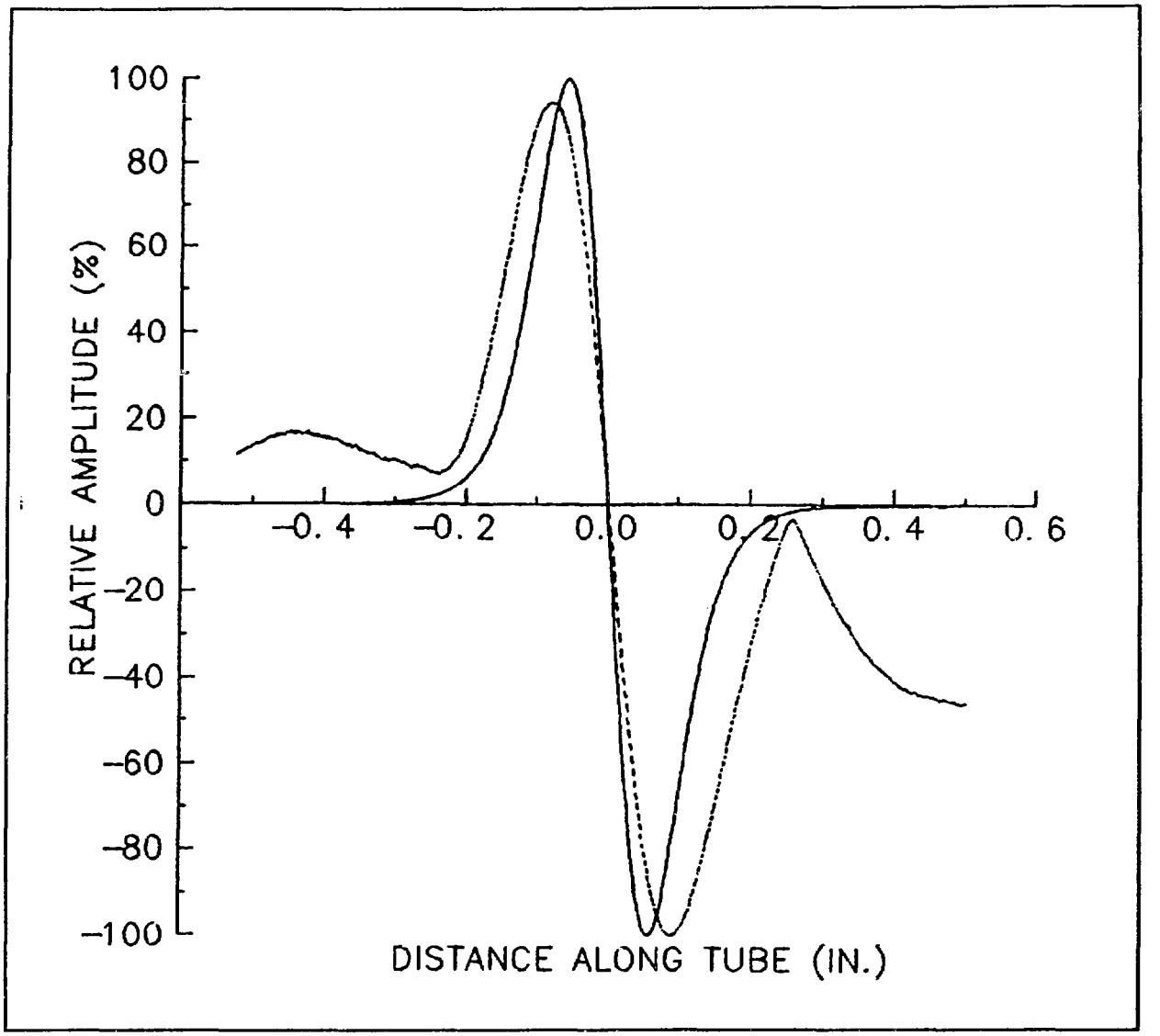

Figure 6 Magnitude of defect signal as a function of distance along tube. The calculated value for a point defect is solid, the measured value for a 40% defect is dashed.

that continues on up in frequency, rather than going to zero as the calculated defect does. This is caused by noise, such as probe wobble, instrument noise and digitizing noise, in the experimental measurements. For the best measurements, this high frequency tail should be attenuated by a low-pass filter. All of the defect signal information will be captured with a cut-off frequency of 120 Hz for the 1 ft per second inspection speed. The noise signals above the 120 Hz cut-off will be attenuated. For faster scanning speeds, the cut-off frequency of the low-pass filter should be raised in proportion to the inspection speeds.

An additional consideration is the number of readings taken per inch of tube scanned. In general, this will depend on the shape and size of the probe relative to the tube. An additional consideration is the tube wall thickness which influences the coil-to-coil spacing in the probe The following studies

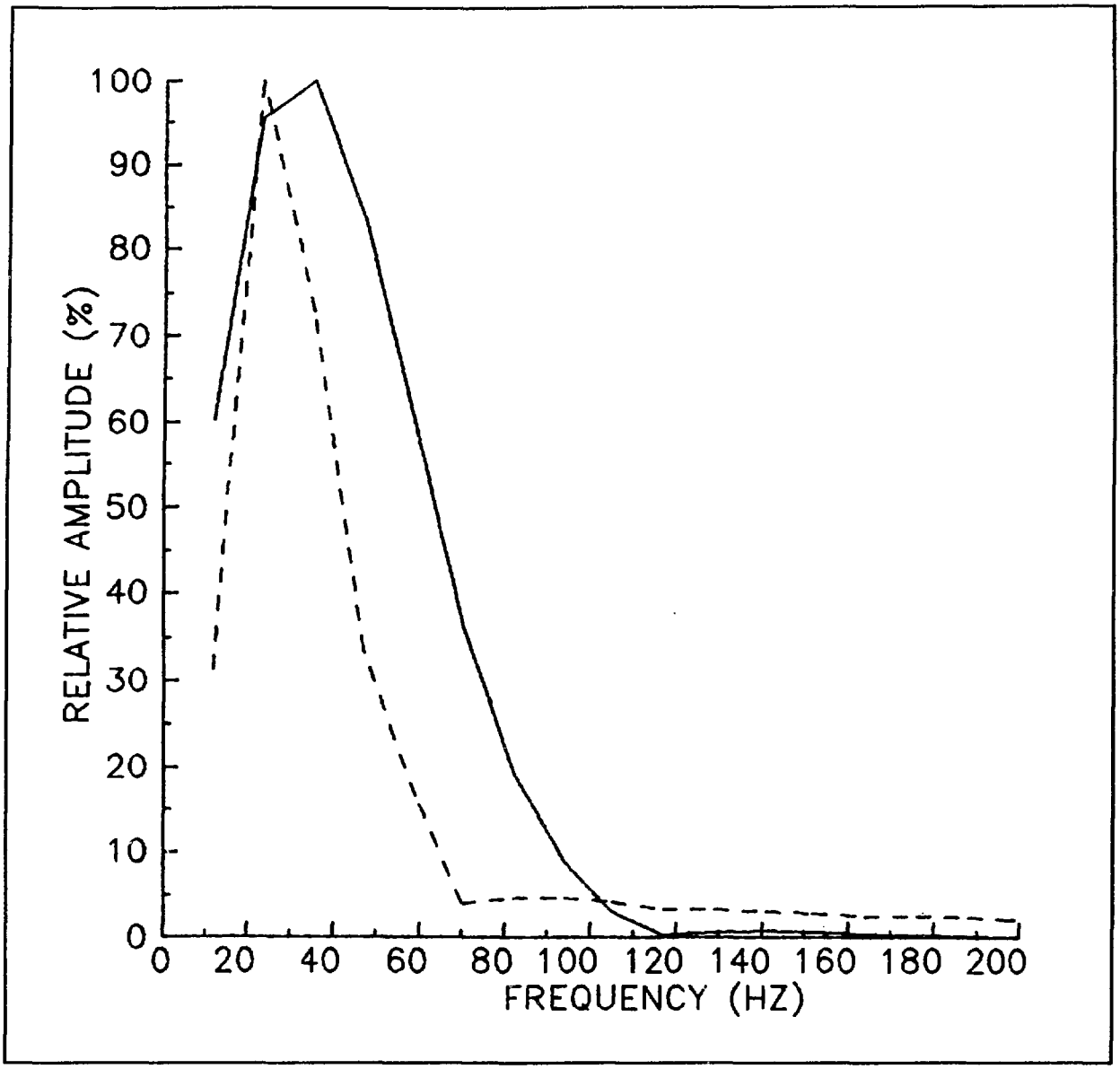

Figure 7 Frequency response of the defect signal as the probe is pulled at a constant speed of a foot per second. The solid curve is calculated for a point defect and represents the maximum frequency response. The dashed curve is for a measured 40% defect.

were performed for a 7/8 in. od tube with a 0.050 in. wall thickness, inspected with a standard Zetec 720 differential bobbin probe. Figure 8 shows the pattern produced as a 40% defect is scanned at a resolution of 100 samples per inch. The resolution is quite good in this case. If, however, the defect is scanned at a resolution of 25 samples per inch, as shown in Figure 9, the resolution is much poorer and the error in sizing the defect increases, depending to some extent on which technique is used to size the defect.

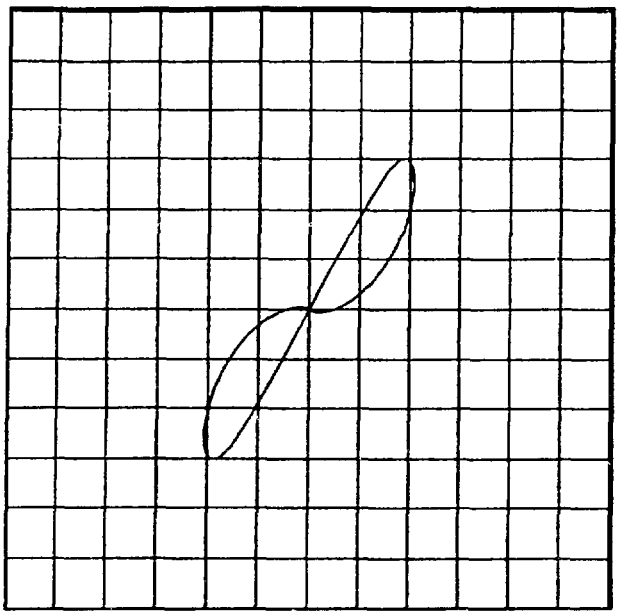

Figure 8 The Lissajous plot is made up of 100 discrete readings per inch. For the plots made up of 25 readings per inch, we can take every fourth reading from this plot.

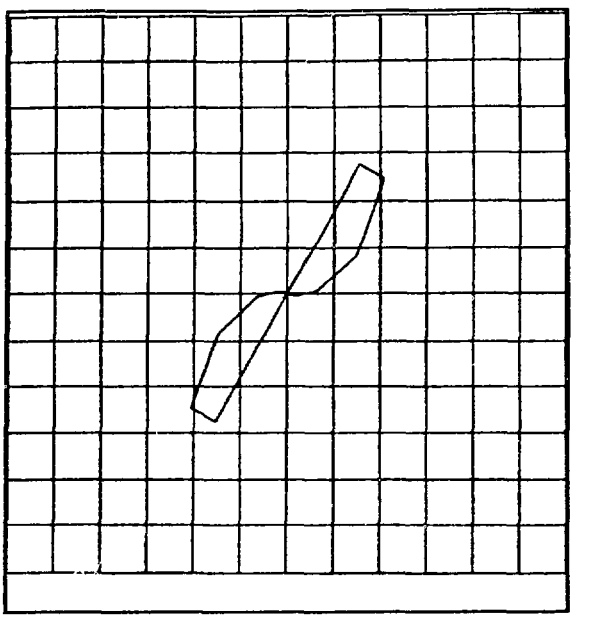

Figure 9 Lissajous plot of a 40% deep defect using 25 readings per inch.

The defect size can be determined using either the maximum slope of the phase or by measuring the phase shift at maximum amplitude. The former method is more accurate for sparse data samples. The sample rate is generally specified as a number of samples per second for a given instrument. This must be converted to the number of samples per inch of tube scanned by dividing by the scan speed used for the test.

In addition, other tube sizes can be approximated from the data shown here by scaling techniques. In general, if we halve the diameter of the tube, tube wall thickness and the probe dimensions, the scan rate in samples per inch would have to be doubled to achieve the same level of sensitivity. The amount of error depends on the depth of the defect and on the number of samples per inch. In Table I we show the variation in the error as a function of these two parameters. Note that the error calculated for the 40% point defect is somewhat greater than that for the experimental defects. This is due to the spread of the signal from the

Table I Possible errors in percent of wall thickness for different sample rates.

DEFECT SIZE (%) SAMPLES PER INCH	100	80	60	40	40Cal
1000	0.00	0.00	0.00	0.00	0.00
500	0.03	0.14	0.19	0.16	0.23
250	0.16	0.21	0.28	0.28	0.46
200	0.18	0.24	0.38	0.25	0.59
100	0.36	0.49	0.83	0.81	1.16
50	0.70	0.91	1.59	1.61	2.31
40	0.92	1.16	2.12	1.98	2.93
25	1.51	1.93	3.11	3.41	6.25
20	1.74	2.26	3.97	3.93	6.47

experimental defects along the tube. The point defect represents the worst case error. The defects in this table are sized using the phase at maximum amplitude, which, as noted above, increases the error. Thus, this table represents the maximum error that may occur for the ASME Section XI defects in bare tubing. Additional studies are underway to determine the error caused by sample rate for defect depth measurements with more complex and mixed signals when other factors such as tube sheets, copper deposits and magnetite deposits are present.

NEURAL NET STUDY

The application of artificial neural networks to the evaluation of eddy-current signals from steam-generator tubes is being investigated under separate funding. The following remarks are intended as a brief introduction to the general nature and present status of this effort.

The term "neural network" has come to have nearly as many meanings as there are students of the field. Nevertheless, the following may be taken as generally representative of the intent. An artificial neural network is a modifiably interconnected set of active, generally non-linear, elements which, in some fashion, accept input signals from the environment, and which both return to the environment some indication of their collective response to these signals and adjust their response to them in a manner which tends to increase the network's capacity for giving unique responses to stimuli with which it has become familiar. The input signals may comprise a pixel by pixel representation of an image, a parametric description of a physical object, a relational description of the time dependent behavior of some system, or the like. For properly prepared networks, the network response will, in the first case, be expressed by the recall, or reconstitution, of one or more of the images the network has previously "learned" and which it finds sufficiently analogous to the presented stimulus. Similarly, the response to a set of parameters will be one of the responses already known for objects described by the same, or nearly the same, set of parameters. The response can be an image, a string of characters or words, an ordered set of control signals, etc. The response to a relational description of some system behavior can be thought of as a path along which the system can be carried, perhaps from one set of operating conditions to a second, while satisfying some set of boundary conditions. These examples only hint at the range of problem types to which neural networks have already been applied. Whatever the application, most artificial networks are designed to capture in their "neural" elements some of the characteristics of the biological neurons which form the building blocks of natural intelligent systems. The more important of these characteristics are noted below.

Reduced to elemental form, the biological neuron may be described in terms of four components. The NERVE BODY (or SOMA) itself is a roughly globular region of 10-80 microns diameter. For our purposes, the nerve body may be considered the source of the nerve impulses via which neurons communicate among one another. These impulses (spikes of millisecond duration) leave the soma along the AXON and, as a result of dense branching of the axon, arrive at receptor sites on as many as 150,000 other neurons. These receptor sites, called SYNAPTIC JUNCTIONS (or simply SYNAPSES), are usually formed, not on the receiving neuron bodies themselves, but on densely branched filamentary extensions of the soma called DENDRITES. The synaptic junctions can be of two general types. An activating junction is one which, upon the arrival of a neuron impulse, leads to an increase in the probability that the receiving

neuron will itself emit an impulse (or fire). An inhibiting junction has the opposite effect. Associated with each of the junction types is a property generally referred to as the Connection Strength, or Weight. The overall effect of an impinging neuron impulse is mediated by this weight. It is because the weights associated with each of the two junction types can, under certain conditions, exhibit a capacity for stimulus-driven alteration that learning can take place.

The artificial neural systems on which our NDE studies are based are derived from the LILARTI schemes of Allen and Schell and represent the most recent in a series of synthetic neural net systems intended from their conception primarily for the purpose of exploring cognition and the degree to which artificial systems can be made to develop and exhibit it. Thus, these systems bear little relation to the products of more conventional work in the area whose structures reflect far more the influence of mathematical rigor than biological reality. Although initially the name of the program which both translated a quasi-biological network definition into a functional network and managed the processing defined by that network, LILARTI has come to refer to that network which, at a given moment, exhibits the most interesting behavior. Although capable of incorporating any combination of members of a nearly limitless spectrum of connectivity classes (most of which are characterized by pseudo-random connectivity within the bounds of their class definitions), the more recent LILARTI systems have shared some characteristic elements. Those associated with the (so far always present) visual system have generally been a small (usually in the range of 31x31 to 101x101 pixel square) "retina", several scene decomposition regions (edge detectors, etc.), outline- or contour map-forming regions, "interesting site" locators, a scene reconstruction region (not altogether inaccurately referred to as a visual cortex), several trainable regions for a learned hierarchy of scene abstractions, and regions whose neurons function very much like the often damned (and, indeed, biologically unlikely) "grandmother cells". A second input sense (referred to, whatever the data source, as the keyboard) serves a broadly analogous set of neural regions. It is the trainable interaction between and among the higher level elements of two (or, in general, several) sensory subsystems which is principally responsible for the more interesting characteristics of a LILARTI wiring. Of the several unusual features of the LILARTI systems, three are of particular importance here. First, and earliest to be incorporated, is the capacity for interaction and contextual learning among the various senses, an attribute which, it is hoped, will ultimately justify the rather grand and early assigned term, "cognitive complementarity". Arising naturally from the concept of cognitive complementarity are the linked notions of the formation of generalized abstractions of features neurally derived from input data and the formation of a related grammar therefrom. Even for the relatively simple neural systems so far explored, these properties have emerged in a natural manner and lend themselves effectively to those applications for which some sort of interface between a system's representation of its actions and a human's representation of his is required.

For our present purposes, this interaction exhibits itself as a capacity for describing to a user the characteristics of the eddy-current signals with which it is presented. These signals are Lissajous patterns obtained at two frequencies, each presented at two different scales to the "retina" of the neural system so that, in effect, the neural system "sees" four representations of flaw signals simultaneously. This simultaneity of presentation leads naturally to

a learning mechanism by which the system discovers what portions of the separate signals can usefully be related in order to produce the most nearly singular description of the presented flaw and to discriminate flaw signals from signals produced by such perturbing influences as tube supports, magnetite deposits, and the like.

Figure 10 illustrates a typical single frequency signal produced when a defect is near the tube support. The defect is the small signal Lissajous pattern with the large tube support signal superimposed. As the relative position of the defect is moved with respect to the tube support, the tube support signal can mask the much smaller defect signal. Magnetite and copper signals can be considerably larger than the tube support signal. In Figure 11 we see the same signal at a much lower resolution. While the complex image is visible in this particular scan, this is not always the case. The resolution of 101 X 101 is slightly above the practical limit of the size of the neural network with the available memory in our computer.

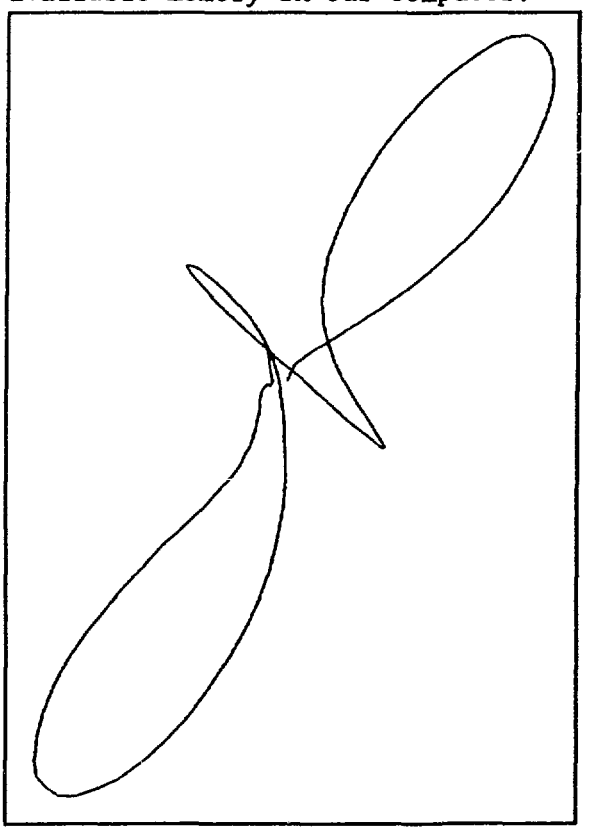

Figure 10 Scan of a 40% OD defect located 0.1 in from center of tube support, made at 500 KHz, 1350 X 1350 resolution.

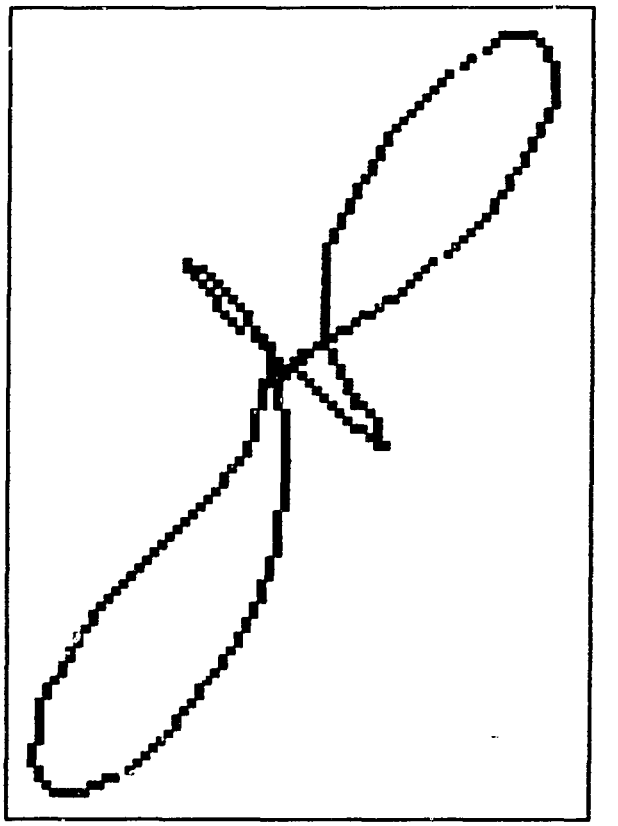

Figure 11 Scan of a 40% OD defect located 0.1 in from center of tube support, made at 500 KHz, 101 X 101 resolution.

Since the data at one frequency do not contain enough information to give an unambiguous measure of the defect in the presence of other property variations, we have to use multiple frequency data. We therefore used both the 100Khz and 500Khz signals for our analysis. In Figure 12, we show the data at both frequencies. Since we did not have the resolution to show the fine detail near

the center of the plot, we magnified these pixels and showed them to the right of the whole plot.

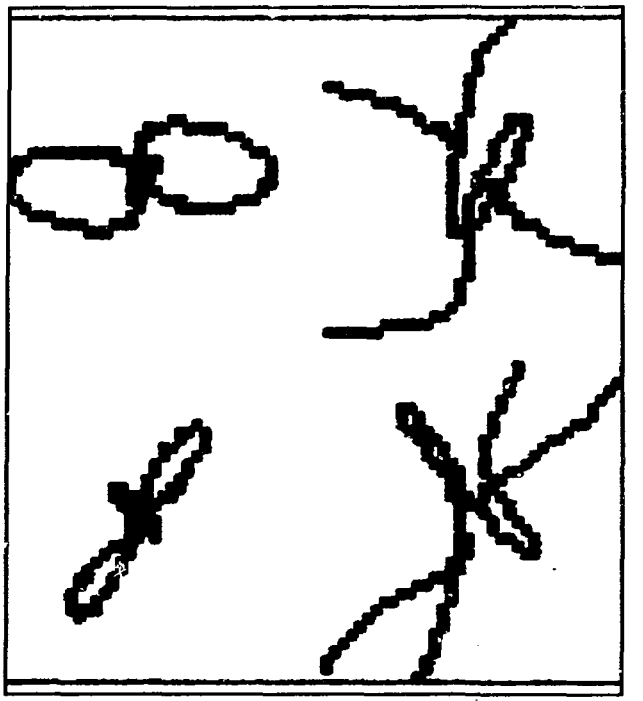

Figure 12 Scan patterns produced by a 40% defect located near a tube sheet at 500KHz and 100KHz. Each part of the image has a resolution of 39 X 39, with an overall resolution of 81 X 81 for the whole picture.

The neural network is presented these pictures for different depth defects that are located at different distances from the tube support, with no mixing to reduce the effects of the tube support. These data were obtained by scans of the ASME Section XI defects, using a MIZ17. To date, results with a still small LILARTI type network comprising about 30,000 neurons and 325,000 connections are promising indeed. The better "tuned" wirings (a representative example of which appears as Figure 13) have yielded overall error rates below 5% when trained with no more than 40 composite signals, or "quartets", over training times which, given that the system runs on a PC clone, are not excessive (of the order of 12 hours). Although our present studies involve flaw evaluation in the presence of only one variable perturbation (distance from the tube support), it is feasible, within the context of the present computing environment, to extend the neural system sufficiently to permit flaw evaluation in the presence of two additional perturbing influences (probably copper and magnetite deposits on the outer surface of the tube). If this extension can indeed be fit into the confines of the present 16 Megabytes of PC memory, and if the processing time is not unduly compromised thereby, we shall attempt to train the system to the degree required to perform flaw size determinations in the presence of any combination of the three perturbing influences. If this effort succeeds, we will retrain the system on the "raw" data signals from the EPRI Level II Data Evaluator training tapes and determine if the network can pass the Level II Inspector's test and thus be qualified for data evaluation.

Extensions much beyond those just noted will inevitably require considerably more computing speed and more memory. One of the most important of these extensions is the increasing of system resolution so that the rescaling aspect of the "quartet" presentation of data can be avoided. We would, of course, maintain the capacity for simultaneous examination of data obtained at two or more frequencies as is it clear from other studies that single frequency measurements cannot lead to unambiguous flaw descriptions in the presence of numerous perturbations (many of which produce, in any case, signals larger than those due to the flaw whose detection and evaluation is desired). This first extension, and one or two less demanding ones as well, would require no more than an order of magnitude increase in processing speed and a factor of four increase in memory and can almost certainly be evaluated in the generation of personal computers

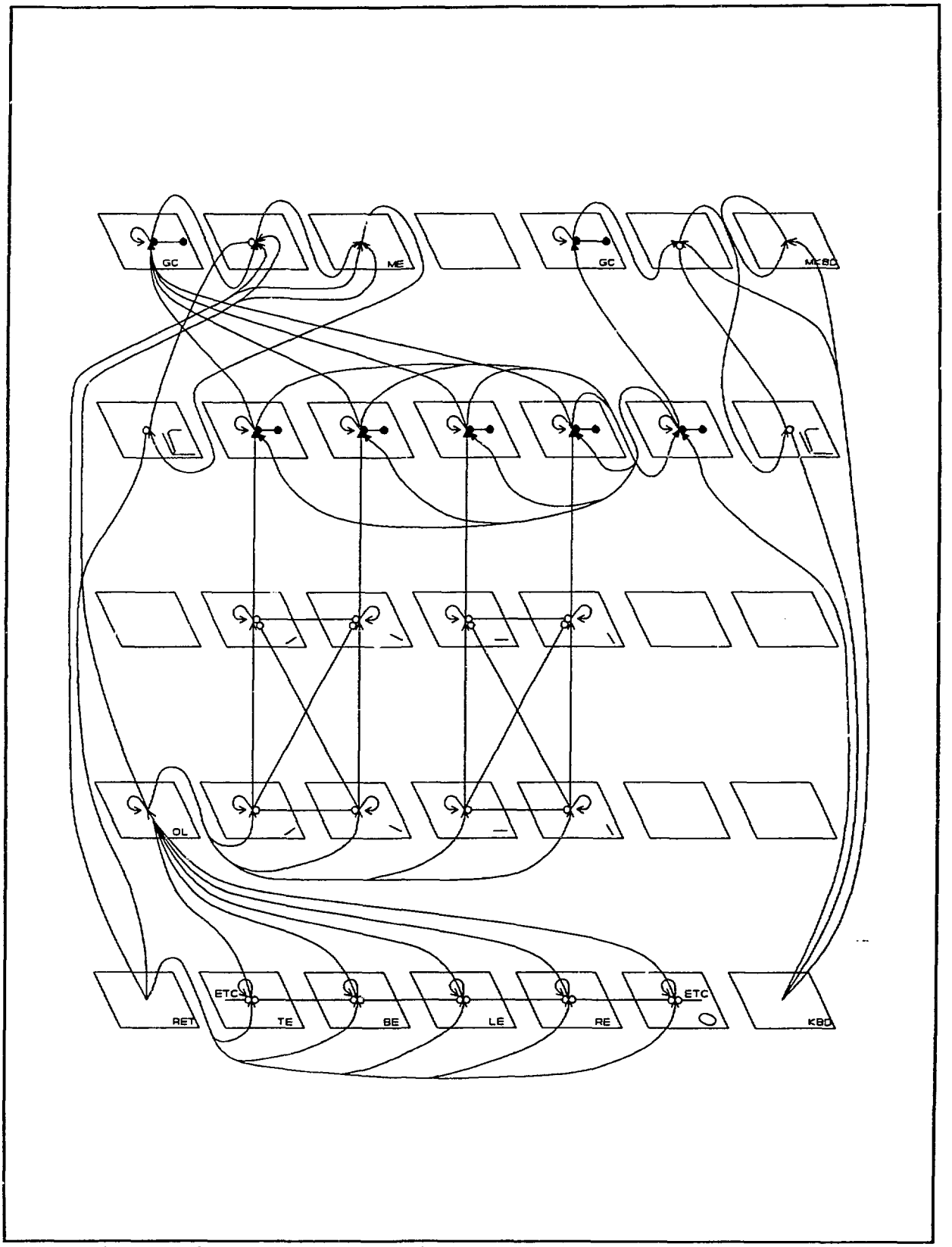

Figure 13 The Lilarti Neural Network for Evaluation of Eddy-Current Signals

just now beginning to appear. Longer term goals include extensions of the developing techniques into such NDE areas as Ultrasonic Testing and Two-Dimensional X-ray imaging and could most effectively be explored in the context of dedicated architectures not unlike those with which we already have some considerable experience.[3,4,5,6]

We conclude this section with two observations. First, present eddy-current data evaluation practice requires that two independent analyses be performed on the data. If we succeed in meeting our near-term goals, it would not be unreasonable to suggest that one of these independent analyses be performed by the multiple-property technique already well explored and that the other be performed by a well trained neural network system. Certainly, the two approaches should be seen as complementary, not competitive.

Finally, it is worth noting that the resolution problem associated with the neural network studies is somewhat analogous to the sample rate problem discussed earlier, an analogy not unrelated to the similarity between the data of Figures 9 and 12. Although we cannot translate the results of one study directly into the domain of the other, the data we have obtained (and continue to obtain) for the neural network studies can be applied directly in the study of sample rate effects in the presence of complex properties.

SUMMARY AND CONCLUSIONS

The power of computerized analysis and synthesis routines for investigation and optimization of complex physical considerations in eddy-current inspection problems for steam generator tubing has been illustrated with several examples. Development of computer codes and applications is ongoing, and a collection of proven codes has been published.[1] Computed aided system design and data analysis can be expected to play a much greater role in steam generator inspection as the process becomes more complex and new degradation modes demand more definitive data. Best and most cost-effective solutions to inspection problems are expected to require significant ongoing efforts based on the work that has already been done.

---

[3] Philip L. Butler, *Design and Implementation of a Parallel Processing Machine for Artificial Intelligence Applications*, Philip L. Butler, Master's Thesis, University of Tennessee, December 1987.

[4] P. L. Butler, J. D. Allen, Jr., et al., *Parallel Architecture for OPS5*, pp. 452-57 in 15th Annual International Symposium of Computer Architecture, Honolulu, Hawaii, May 30-June 2, 1988, IEEE.

[5] P. L. Butler, J. D. Allen, Jr., *Design and Implementation of a Parallel Computer for Expert System Applications*, pp 638-45 in Applications of Artificial Intelligence VI, ed. Mohan M. Trivedi, SPIE.

[6] Winner R&D-100 Award, 1988.